Thermal Stability and Flammability of Banana-Fiber-Reinforced Polypropylene Nanocomposites

Manoranjan Biswal, Smita Mohanty, Sanjay K. Nayak

Laboratory for Advanced Research in Polymeric Materials, Central Institute of Plastics Engineering and Technology, Bhubaneswar, Orissa 751024, India

Received 16 November 2010; accepted 11 July 2011
DOI 10.1002/app.35246
Published online in Wiley Online Library (wileyonlinelibrary.com).

ABSTRACT: Banana-fiber-reinforced polypropylene nanocomposites were prepared with a melt-blending technique followed by compression molding. The thermal stability and fire retardancy of the fiber-reinforced nanocomposites was studied as a function of the variable weight percentages of fibers and nanoclays with both thermogravimetric analysis (TGA) and cone calorimetry measurements. The test results indicated char formation at relatively low loadings of the nanoclays, thereby indicating flame retardancy in the fiber-reinforced nanocomposites. The change in the degradation pathway of the polymer was observed with the incorporation of clay within the natural-fiber-reinforced composite, wherein the clay layers acted as barriers to mass transport that contributed to superheated conditions in the condensed phase. TGA thermograms also revealed improved thermal properties compared with the virgin matrix. Both the isothermal and nonisothermal degradation kinetics of the fiber-reinforced nanocomposites were also studied. Differential scanning calorimetry studies showed an increase in the melting and crystallization temperatures of PP in the fiber-reinforced nanocomposites. Furthermore, the morphology of the fiber-reinforced nanocomposites was evaluated with X-ray diffraction and transmission electron microscopy, respectively. J Appl Polym Sci 000: 000–000, 2012

Key words: nanocomposites; poly(propylene) (PP); TEM; thermal properties

INTRODUCTION

Fiber-reinforced composites have generated considerable interest, both in terms of industrial applications and fundamental research in recent years.[1–4] Lignocellulosic natural fibers, such as flax, cotton, hemp, jute, sisal, kenaf, pineapple, ramie, bamboo, and banana, provide unique opportunities for their utilization in the fabrication of inexpensive composite materials. The combination of their unique mechanical and physical properties together with their ecofriendly characteristics have encouraged application in several industrial sectors, including aerospace, automotive, building, and construction. The performance characteristics of a fiber-reinforced composite predominantly depend on the fiber/matrix interfacial bond strength. The matrix layer in contact with the fiber surface has different properties from the bulk matrix because of the fiber/polymer interactions due to the mechanical matrix immobilization of the chains, electrostatic forces, or chemical bonds in the presence of internal stresses, voids, or microcracks within the interlayer. However, several impediments of natural fiber composites, such as hydrophilicity in the fibers, limited processability, and incompatibility with the polymer matrix, have been the primary reason for the penetration of these materials in niche markets. Surface modification of the fibers with various methods has been proposed to improve the compatibility between the lignocellulosic natural fiber and the polymer matrix. Several studies on the use of coupling agents/compatibilizers, sizing agents, modifiers, plasma treatment, chemical modification through grafting, mercerization, and acetylation have been done by various authors to modify the interface between the lignocellulosic natural fibers and the polymer matrix.[5–7]

Thermal degradation of natural fibers has been a crucial factor for the development of natural fiber composites. The curing temperature in the case of thermoset and extrusion temperatures in thermoplastic-based composites has been a vital element in the determination of the thermal stability of the meterials.[8] Extensive investigation of the dynamic mechanical and thermal stability of jute/polypropylene (PP) composites by Mohanty and coworkers[9–11] revealed an improved fiber/matrix interface with the incorporation of maleated polyolefins. Several studies pertaining to the stability of lignocellulosic natural fibers have also been investigated by authors in different systems, such as jute/PP, sisal/PP, and banana-/glass-fiber hybrid composites. Also, variations in the thermal stability in these natural fiber

Correspondence to: S. K. Nayak (drsknayak@yahoo.com).

composites as a function of temperature under static and dynamic conditions have been demonstrated by various workers.[12,13] As per our earlier work on the mechanical and thermal behaviors of PP/pineapple-leaf-fiber nanocomposites, the incorporation of pineapple leaf fiber within the PP nanocomposite matrix enhanced the thermal stability of the system.[14]

PP/clay nanocomposites have been the subject of research because of their significantly enhanced macroscopic material properties compared with traditional fillers.[15–18] PP, a nonpolar polymer, is a versatile thermoplastic used for many high-end applications. Polyolefin nanocomposites have gained considerable commercial viability for automobile applications because of their low density and high modulus. The presence of a third component, namely, a compatibilizer, required to facilitate the intercalation of PP within the clay galleries, has been widely reported. Several investigations have confirmed that the presence of a compatibilizer with polar groups, such as maleic anhydride grafted polypropylene (MA-*g*-PP), is necessary to obtain a significant improvement in the properties of the nanocomposites.[19] The outstanding properties of polymer/clay nanocomposites, including a large surface area, high aspect ratio, and good interfacial interaction with the polymer matrix, primarily depend on the structural nature of the clay; these factors are essentially observed in exfoliated nanocomposites.[20]

Nanocomposites based on these phase systems containing nanoclay, fibers, and a polymer matrix have not been widely explored. An extensive literature survey indicated that the effects of natural fibers on the thermal and flammability characteristics of PP nanocomposite systems need to be investigated. However, there exist some hypotheses that indicate that the introduction of fiber into the polymer/clay system can satisfactorily enhance the reinforcing effect with increased mechanical and thermal properties. Lei et al.[21] reported that in case of high-density polyethylene/pine/clay nanocomposites, there was every possibility of counteraction between the two different fillers, that is, the nanoclay and fibers, which might have had some negative impact on the performance of the system. The authors claimed that the incorporation of high-molecular-weight or higher acid number MA-*g*-PP could have possibly enhanced the nanocomposite performance because of the formation of the interface. Thus, fiber-reinforced nanocomposites can be used in the automotive, structural, and aerospace areas, wherein the performance, along with the cost effectiveness, is crucial for various end-use applications.

In this investigation, variation in the thermal and flammability properties of PP nanocomposites as a function of banana-fiber loading was examined. The corresponding heat loss, mass loss, time of ignition, and specific extinction area (SEA) in the virgin matrix, PP nanocomposites, and fiber-reinforced nanocomposites are discussed. Also, an elaborative discussion on the degradation kinetics of different materials is given. Furthermore, the fiber-reinforced nanocomposites samples were also subjected to scanning electron microscopy (SEM) and transmission electron microscopy (TEM) analysis to evaluate the fracture surface and interfacial adhesion morphology. The thermal stability in the samples was also studied with differential scanning calorimetry (DSC) and thermogravimetric analysis (TGA).

EXPERIMENTAL

Materials

Isotactic PP (H110MA), having a melt flow index of 11 g/10 min and a density of 0.91 g/cc and obtained from Reliance Industries (Mumbai, India), was used as the base polymer matrix. Cloisite 20A (C20A), organically modified montmorillonite with dimethyl dihydrogenated tallow quaternary ammonium, having a cation exchange capacity of 95 mequiv/100 g of clay, and procured from Southern Clay Products (Gonzales, TX), was used as the nanoclay. EpoleneVR G-3003, having a density of 0.91 g/cc and a molecular weight of 26,000, was procured from Eastman Chemicals (Cologne, Germany), was used as a compatibilizer. Banana fiber was obtained from Sheeba Fibers and Handicrafts (Poovancode, India) and was used as a reinforcing agent. The physical and mechanical properties of the banana fiber are represented in Table I.

Preparation of the banana-fiber-reinforced polypropylene (BRPP) nanocomposites

The banana fibers were cut to 50 cm in length and were soaked in a 5% NaOH solution at 30°C for 2 h to remove dirt and other impurities. Subsequently, the fibers were washed several times with distilled water, neutralized with dilute acetic acid, and finally washed again with distilled water. The final pH was maintained at 7. The fibers were then dried at room temperature for 48 h; this was followed by oven drying at 100°C for 6 h to remove the moisture and volatiles. To ensure easy blending of the fibers with the matrix, the fibers were cut to a fiber length of about 6 mm, with an electronic fiber-cutting machine.

Compounding was carried out with a melt mixer (Haake Rheocord 9000, Haake, Karlsruhe, Germany) having two Banbury rotors and a mixing chamber with a 69-cm^3 volumetric capacity. In the first stage, PP nanocomposite containing different weight percentages of C20A nanoclay (1, 2, and 3%) and 5 wt % MA-*g*-PP were prepared with a melt-interaction

TABLE I
Physical and Mechanical Properties of the Banana Fiber

Property	
Width or diameter (μm)	80–250
Density (g/cm^3)	1.35
Microfibrillar angle (°)	11
Cellulose/lignin content (%)	65/5
Elastic modulus (GN/m^2)	8–10
Tenacity (MN/m^2)	529–754
Elongation (%)	1.0–3.5

technique at a temperature of 180°C at a mixing speed of 40 rpm for a duration of 15 min. In the second stage, an MA-*g*-PP clay master batch was melt-blended with different weight percentages of banana fibers (10, 20, and 30%) at a screw speed of 45 rpm for 15 min at 190°C.

Finally, these premixes were brought to room temperature and compression-molded with a Delta Malikson Pressman 100T compression-molding machine (Mumbai, India) at 190°C to produce sheets 3 ± 0.1 mm in thickness.

Mechanical properties

The tensile properties were measured as per ASTM D 638 with a gauge length of 50 mm at a crosshead speed of 50 mm/min with a universal testing machine (LR 100 K, Lloyds Instruments, Fareham, United Kingdom). The flexural properties were measured as per ASTM D 790 with a gauge length of 50 mm at a crosshead speed of 1.3 mm/min with the same universal testing machine. The data reported are the averages of 10 specimens for each test with corresponding standard deviation values.

Flammability measurements

A cone calorimeter (FTT, East Grinstead, United Kingdom) was used to measure the ignition characteristics, heat release rate (HRR), and sample mass loss in accordance with ISO 5660. An external radiant heat flux of 50 kW/m^2 was applied. All of the samples were measured in the horizontal position and wrapped with thin aluminum foil except for the irradiated sample surface. The standard uncertainty of the measured HRR was ±10%. The peak HRR, mass loss rate (MLR), and SEA data were measured at 50 kW/m^2.

TEM

Ultrathin sections of the nanocomposites with thicknesses of about 50–70 nm were microtomed at room temperature with a Leica Ultracut UCT microtome (Leica, Wetzlar, Germany) equipped with a diamond knife. Subsequently, the samples were subjected to TEM analysis with a transmission electron microscope (JEOL-1200 EX, Japan) at an acceleration voltage of 80 kV without any chemical staining.

SEM

The SEM of tensile fractured composite specimens was carried out with a JEOL-JSM T330A (Eching, Germany). The samples were sputter-coated with platinum and dried for 0.5 h at 70°C *in vacuo* before study.

Thermal properties

The melting, crystallization, and thermal stabilities of the virgin PP, PP nanocomposite, and fiber-reinforced PP nanocomposite samples were studied with DSC (PerkinElmer Diamond DSC, Waltham, Massachusetts, USA) and TGA (PerkinElmer Pyris-7 TGA, Waltham, Massachusetts, USA).

DSC analysis was carried out with 5–10-mg samples at a scanning rate of 20°C/min at a temperature of 30–200°C under a nitrogen atmosphere. The corresponding melting temperature (T_m), heat of fusion (ΔH_m), and crystallization temperature (T_c) were recorded.

Approximately 5–10-mg samples were taken for TGA; these were scanned from 40 to 600°C at a heating rate of 20°C under a nitrogen atmosphere to evaluate the peak temperature from the differential thermogravimetry (DTG) curve. Furthermore, the samples were also subjected to isothermal and nonisothermal conditions to study the activation energy (E_a) at each stage. The initial and final degradation temperature and corresponding percentage weight loss for the samples were noted.

RESULTS AND DISCUSSION

Effect of the nanoclay and MA-*g*-PP on the mechanical properties of the PP nanocomposites

The mechanical properties of the nanocomposites determined as a function of clay content (1, 2, or 3 wt %) with 5 wt % MA-*g*-PP are represented in Table II. It was evident that incorporation of 3 wt % nanoclay and 5 wt % MA-*g*-PP showed the optimum increase in the mechanical strength. Increases of 40.82% tensile strength and 45.67% flexural strength were obtained compared with the values for the PP matrix. Similarly, the tensile and flexural moduli also showed linear increases with increasing clay content. This increase in the properties of the matrix polymer was due to the insertion of the polymer chains inside the silicate clay layers; this led to an increase in the surface area of interaction between the clay and polymer matrix.[22] Additionally, the

TABLE II
Mechanical Properties of the PP, PP Nanocomposites, and BRPP Nanocomposites

Sample	Sample abbreviation	Tensile strength (MPa)	SD	Tensile modulus (MPa)	SD	Flexural strength (MPa)	SD	Flexural modulus (MPa)	SD	Impact strength (J/m)	SD
Pure PP	PP	18.52	1.2	946.78	17	56.7	2.8	1580	18	19.20	1.1
PP/clay/PP-*g*-MA (94/1/5)	—	22.52	0.9	1094.5	22	67.9	2.5	2340	10	23.85	0.9
PP/clay/PP-*g*-MA (93/2/5)	—	23.95	1.6	1187.3	15	72.6	2.4	2590	11	27.92	1.4
PP/clay/PP-*g*-MA (92/3/5)	OPP	26.17	2.2	1272.4	21	82.6	3.2	2990	24	20.32	0.9
OPP/10 wt % MBF	BRPP-10	27.04	1.6	1568.01	22	87.82	2.6	3287	26	21.93	0.6
OPP/20 wt % MBF	BRPP-20	29.44	1.2	1937.82	19	92.60	2.2	3824	22	22.59	0.8
OPP/30 wt % MBF	BRPP-30	33.28	1.8	2562.06	23	95.72	3.8	5836	36	26.32	1.2
OPP/40 wt % MBF	BRPP-40	30.22	1.2	1856.12	18	93.64	2.1	5244	12	24.62	1.3

The clay content and MA-*g*-PP were fixed to 3 and 5 wt %, whereas the fiber content was varied from 10 to 40 wt %. SD, standard deviation; MBF, mercerized banana fiber. The OPP nanocomposites were at 92/3/5 PP/clay/PP-*g*-MA.

incorporation of MA-*g*-PP as compatibilizer facilitated expansion of the gallery space of the reinforcing nanoclay by the inclusion of polar groups to intercalate between the clay layers through hydrogen bonding with the oxygen groups of clay tetrahedral.[23–27] Furthermore, we also observed that there was no substantial increase in the impact strength; this was possibly due to the presence of clay agglomerates, which resulted in nonuniform dispersion within the polymer matrix.[28] Because the nanocomposites prepared with 3 wt % nanoclay (C20A) with 5 wt % MA-*g*-PP [optimized polypropylene (OPP)] showed optimum tensile and flexural strengths, this composition was retained for further investigation to fabricate the BRPP nanocomposites.

Effect of the fiber loading on the mechanical properties of the BRPP nanocomposites

The mechanical properties of the BRPP nanocomposites at variable weight percentages of fiber loading are shown in Table II. The test results indicated a linear increase in the mechanical properties of the nanocomposites with an increase in the fiber loading from 10 to 30 wt %. OPP in combination with 30 wt % banana fiber (BRPP-30) exhibited an improved tensile strength of 33.28 MPa with a flexural strength of 95.72 MPa. Increases of approximately 79.69% in the tensile strength and 40.76% in the flexural strength compared with those for the virgin PP were obtained. The presence of 5 wt % MA-*g*-PP in the fiber-reinforced nanocomposites also contributed to a significant improvement in the mechanical properties. MA-*g*-PP acted as a dispersing agent between the polar fibers and nanoclay within the nonpolar thermoplastic matrix; this resulted in improved interfacial adhesion. Also, as confirmed by our earlier investigation, the anhydride groups of MA-*g*-PP formed an ester linkage with OH groups of fibers. In this case, MA-*g*-PP balanced the interfacial interaction in both banana fibers and C20A; this thereby mediated the polarity and increased the stress transfer from the matrix to the filler. Furthermore, the high-molecular-weight MA-*g*-PP had more flexible PP chains; these were able to diffuse into the matrix; this led to interchain entanglements and, thus, contributed to the mechanical continuity of the system.[29] However, an increase in the MA-*g*-PP content to 7 wt % resulted in a decrease in the mechanical strength of the composites; this was in accordance with the results reported by Mohanty et al.[30] for jute-reinforced poly(ester amide) composites. This was probably due to self-entanglement among the compatibilizer chains rather than with the polymer matrix and resulted in slippage. Thus, 5 wt % MA-*g*-PP was taken into consideration for further studies. The deterioration in tensile strength at higher fiber contents of 40 wt % was a direct consequence of the poor fiber/matrix adhesion, which led to microcrack formation at the interface under loading and nonuniform stress transfer due to the fiber agglomeration in the matrix. Higher weight percentages of fiber contents also led to an increase in fiber–fiber interaction and resulted in difficulties in the dispersion of the fibers within the polymer matrix.

SEM

The SEM micrographs of the BRPP nanocomposites with 30 wt % banana fiber (Fig. 1) showed that the fibers embedded within the polymer matrix were well dispersed. The fiber pullout, together with the PP matrix during fracture in tensile testing, indicated better cohesive coupling between MA-*g*-PP, the fibers, and the PP matrix; this revealed efficient fiber–matrix adhesion. It also confirmed that the compatibilizer adhered to the primary cell wall of the banana fiber and that the crack did not run through the fiber–matrix interface or perpendicular to the fiber and was fully split over the fiber length. This was probably due to the anhydride group present in MA-*g*-PP, which strongly adhered to the

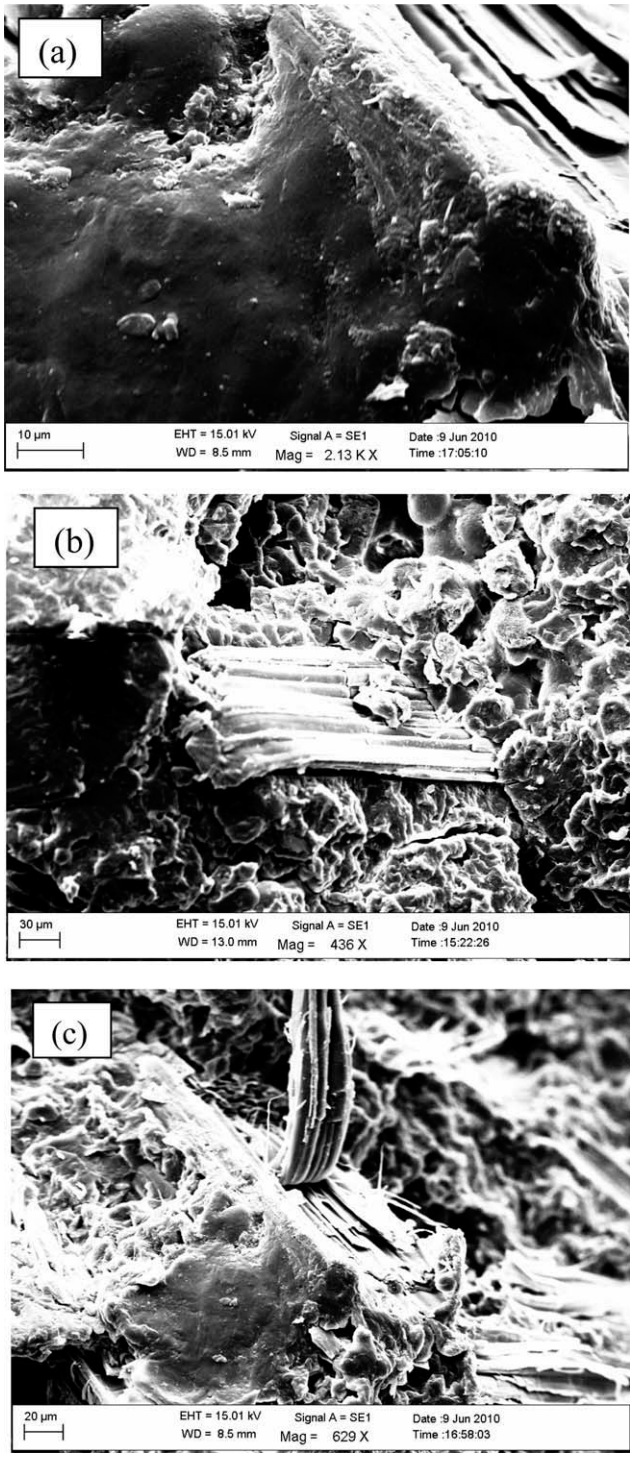

Figure 1 Scanning electron micrographs of the brittle-fractured BRPP-30 nanocomposites at different magnifications.

—OH groups present on the banana fiber surface; this confirmed the fact that the fracture did not occur at the interface but at the fiber itself. A homogeneous distribution of nanoparticles in the PP matrix was achieved, although some agglomeration of particles was observed on the surface. However, SEM micrographs of the banana-fiber-reinforced nanocomposites with MA-*g*-PP did not provide any phenomenal morphological change because of the dispersion of the nanoclay within the composite matrix. Hence, TEM analysis of the nanocomposites samples could have possibly substantiated the dispersion of the clays within the banana-fiber-reinforced PP nanocomposite system.

TEM

The arrangement of clays within the OPP and BRPP-30 nanocomposites was studied with transmission electron micrographs, as depicted in Figure 2. TEM micrographs of the OPP nanocomposites indicated both thick dark and thin gray strips. The dark strips, which may have consisted of stacks of silicate layers, indicated the breakup of the clay tactoids. On the other hand, the gray lines, which may have represented a single layer or small stacks of clay platelets, indicated a state of complete exfoliation within the matrix. The thin gray lines thus represented clay nanolayers within the resolution provided. In the case of banana-fiber-reinforced nanocomposites, exfoliated clay galleries, along with banana fiber microfibrils adhering to the PP matrix, were observed. Also, the regions of intercalated layers were seen in micrographs; these indicated improved interfaces between the fiber, nanoclay, and PP due to the formation of chemical/physical bonds.

X-ray diffraction (XRD)

The XRD patterns of the C20A, OPP, and BRPP-30 nanocomposites are shown in Figure 3. The d_{001} spacing was calculated from the peak positions with Bragg's law: $n\lambda = 2d \sin\theta$, where λ is the X-ray wavelength (1.54 Å) and d is the distance between crystallographic planes. The XRD pattern of the modified C20A clay revealed a reflection peak at 3.78°, which corresponded to a *d*-spacing of 23.3 A°. For the PP/clay system with 3 wt % nanoclay and 5 wt % MA-*g*-PP, the (001) peak shifted to a lower angle of 2.84°, which corresponded to a *d*-spacing of 32.08 Å. This indicated an increase in the interlayer distance of clay and revealed an intercalated structure. Furthermore, the XRD patterns of the banana-fiber-reinforced nanocomposites with 30% fiber loading revealed an absence of diffraction peaks within the experimental range; this suggested exfoliation of the clay galleries. This behavior was probably due to the fact that the MA-*g*-PP molecules acted as a compatibilizer and could enter and penetrate into the clay galleries because of stronger hydrogen bonding between the maleic anhydride group of MA-*g*-PP and oxygen groups of C20A at the interface. This strong bonding contributed to an increase in the gallery spacing of clay and, thereby, allowed the PP chains to enter and break the clay galleries during

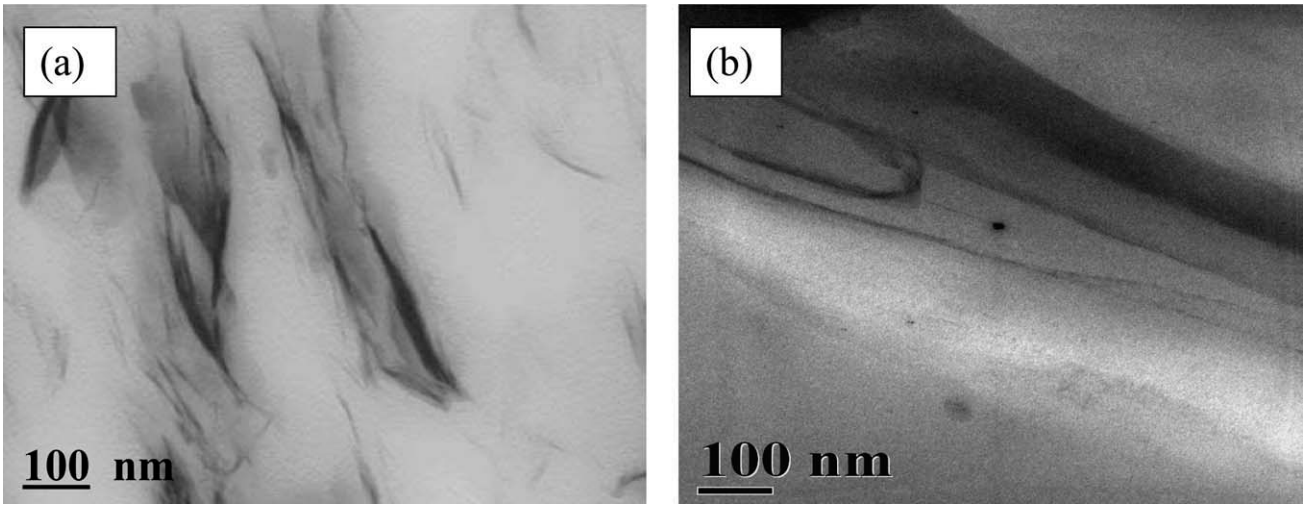

Figure 2 Transmission electron micrographs of the (a) OPP and (b) BRPP-30 nanocomposites at a 100-nm magnification.

compounding. This resulted in an exfoliated and well-dispersed clay structure. Similar results were also reported by Lei et al.,[31] where the interlayer spacing of clay layers increased with the incorporation of pine flour in high-density polyethylene–wood composites. As far as the crystallization behavior was concerned, the addition of 30 wt % fiber did not affect the position of the peaks; however, a decrease in the peak intensity was observed. This suggested the same crystal structure with different values of degree of crystallinity (X_c) within the range 10–25° (Fig. 4). This phenomenon may also have been due to the nucleating ability of the fibers, which accelerated the crystallization process in the PP matrix and in the OPP nanocomposites. However, there was a complication in the analysis of the XRD pattern in the case of the nanocomposites containing natural fibers as compared to the virgin PP and OPP nanocomposites. The presence of hemicelluloses and lignin in natural fibers indicates amorphous regions, whereas cellulose exhibits the characteristics of both amorphous and crystalline regions that have diffraction peaks, which might have overlapped with the peak value of the PP matrix.

Effect of the nanoclay on the flammability properties of the BRPP nanocomposites

The measured HRR curves for the PP, OPP, and BRPP nanocomposites with banana-fiber contents from 10 to 30 wt % are shown in Figure 5 and Table III. It was observed that the maximum HRR for PP was 2498.2 kW/m^2 (curve a), whereas the OPP nanocomposite showed a comparatively lower HRR value of 748.3 kW/m^2 (curve b). This significant reduction in the HRR in the OPP nanocomposites was probably due to the presence of the nanoclay,

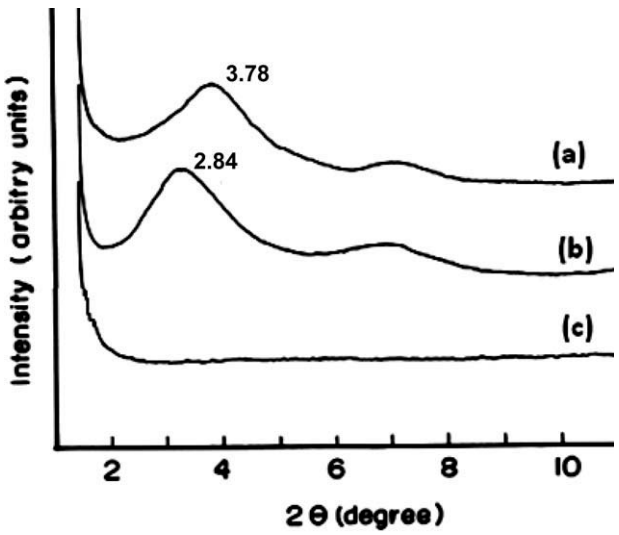

Figure 3 XRD patterns in the region 0–10° for (a) C20A, (b) OPP, and (c) the BRPP-30 nanocomposites.

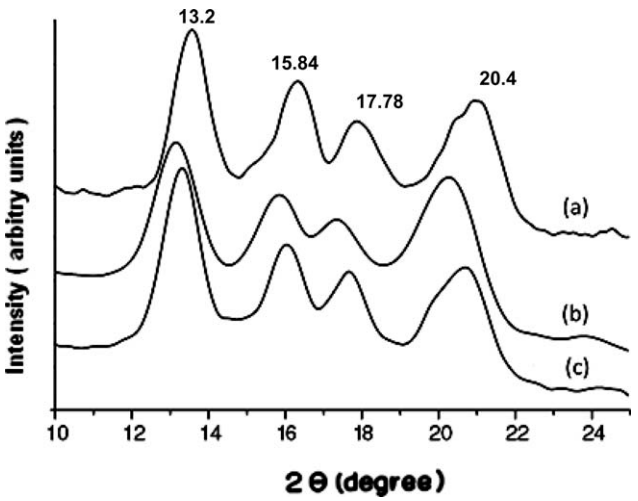

Figure 4 XRD patterns in the region 10–25° for the (a) PP, (b) OPP, and (c) BRPP-30 nanocomposites.

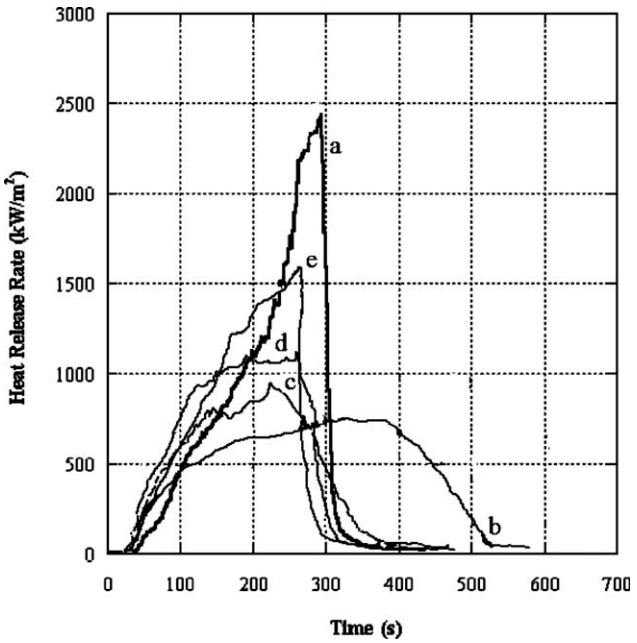

Figure 5 HRRs of (a) PP, (b) OPP, (c) BRPP-10, (d) BRPP-20, and (e) BRPP-30.

which produced a change in the degradation pathway in the polymer matrix and, thus, acted as a barrier by creating a tortuous path for migration.[32] This could also be attributed to a change in thermal properties or an increase in the radiation absorptivity due to the high aspect ratio of the nanoclays.[33] Furthermore, with a comparison of the HRR curves of the OPP and BRPP nanocomposites with virgin PP, it was observed that the fiber-reinforced nanocomposites exhibited different behaviors toward thermal decomposition and combustion characteristics because of the presence of flammable banana fibers. The banana-fiber-reinforced nanocomposite showed a bimodal HRR revealing two distinct characteristic peaks. The initial peak was probably due to the presence of the fiber, which charred and suppressed the heat release in the first stage; this was followed by possible char-surface rupture and burnout of the whole sample in the second stage. Although the presence of banana fibers brought about an earlier ignition of PP, the process of combustion proceeded at a significantly lower HRR and lower MLR. Also, we assumed the presence of lignin and hemicelluloses in the fiber, wherein the lignocellulosic fibers brought about an increase in the levoglucosan formation during pyrolysis. Levoglucosan is considered to be a cellulose monomer, which is usually evolved in the form of extremely flammable fluid tar.[34] E_a of natural fiber pyrolysis increases with increasing X_c; this is mainly possible through fiber treatment with an effective swelling agent.[35] The increased percentage of banana fiber in the OPP nanocomposites indicated a higher value of HRR and smoke release; this showed the typical characteristics of lignocellulosic fibers. However, nanocomposites in the presence of fiber and nanoclay behave differently in fire, depending on their respective thermal stabilities. When the interfacial adhesion is weak, the two phases are pushed apart, where the matrix burns more vigorously and the filler no longer acts as an insulator and sometimes acts rather as a heat conductor and, thus, increases the flammability.[36] Further, the presence of the compatibilizer MA-*g*-PP increased interfacial adhesion and gave a lower value, as expected; this was already confirmed from the morphological studies with SEM, as discussed in earlier sections. Another factor describing the fire-retardant property is MLR. The trends of the measured MLR curves were very close to those of the HRR curves, which were calculated with the time derivative of the measured weight of the PP, OPP, and BRPP nanocomposites, as shown in Figure 6.

Thermal analysis

The thermal degradation behavior of the PP, OPP, and BRPP nanocomposites at various percentages of fiber loading was investigated with TGA and DTG thermograms, as shown in Figures 7 and 8, respectively. It is evident from the figures that the thermal degradation of virgin PP started at 246.2°C, and 100% degradation was noticed at 398°C. However, with the incorporation of nanoclays, there was a substantial enhancement in the thermal stability of the OPP nanocomposites with an initial decomposition peak at 384°C and a final decomposition peak

TABLE III
Cone Calorimetric Parameters for the PP, OPP, and BRPP Nanocomposites

Description	PP	OPP	BRPP-10	BRPP-20	BRPP-30
Time to ignition (s)	30	36	28	27	26
Time of flameout (s)	561	855	719	648	615
Total heat release (MJ/m^2)	100.5	107.3	121.7	137.4	141.5
Mass lost (g)	30.8	31	32.5	32.2	32.6
HRR (kW/m^2)	2498.2	748.3	926.4	1136.77	1256.2
Total smoke release (m^2/m^2)	1298.8	1164.5	1581.9	1746.5	1612.7
SEA (m^2/kg)	445.87	519.61	304.1	322.24	360.42

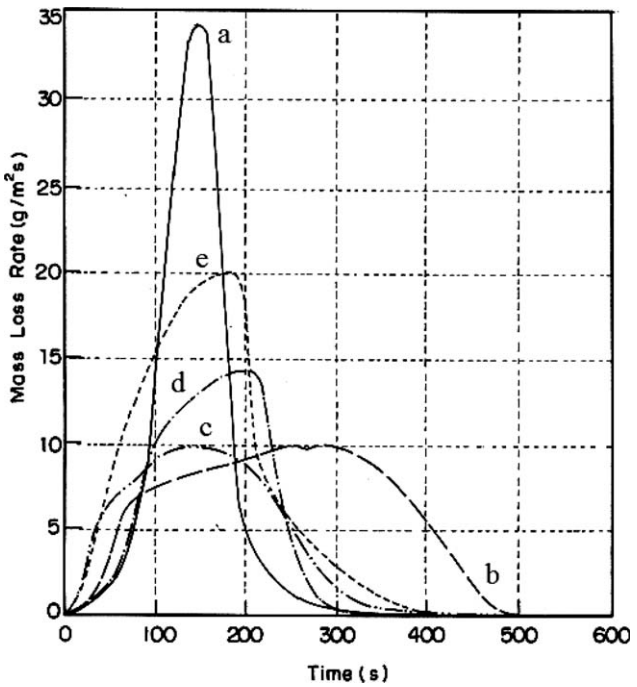

Figure 6 MLRs of (a) PP, (b) OPP, (c) BRPP-10, (d) BRPP-20, and (e) BRPP-30.

at 452°C; this gave a charred residue of 2.8%. The increase in the thermal stability of the nanocomposites was attributed to the organic/inorganic interaction between the polymer and nanoclays, wherein the organoclay delayed volatilization of the products generated at the temperature of carbon–carbon bond scission of the polymer matrix.[37–40] Furthermore, the incorporation of banana fiber within the PP nanocomposite matrix resulted in a different thermal degradation tendency. The DTG curves indicated a two-step degradation, in which the initial degradation at 340–360°C was probably due to dehydration from the cellulose unit and thermal cleavage of glycosidic

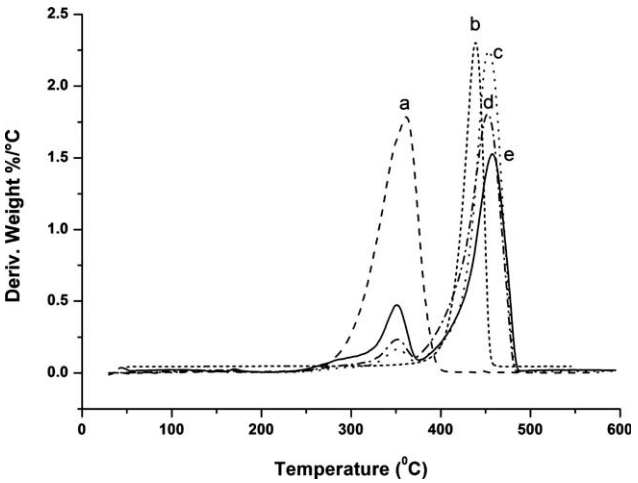

Figure 8 DTG curves of (a) PP, (b) OPP, (c) BRPP-10, (d) BRPP-20, and (e) BRPP-30.

linkages by transglycosylation and scission of C—O— and —C—C— bonds. The second decomposition occurred at 420–480°C; this was attributed to aromatization, involving the dehydration reaction and giving a weight loss of about 88%.

Isothermal degradation kinetics

The catalytic decomposition and barrier effect of the silicate layers were clearly evident from the isothermal thermogravimetric curves, as shown in Figure 9 for the virgin PP, OPP, and BRPP nanocomposites at 300°C for 30 min in a nitrogen atmosphere. The thermal stabilities of the OPP nanocomposites were found to be higher compared to that of virgin PP. The OPP nanocomposites showed a delayed decomposition compared to virgin PP because of the homogeneous distribution of the nanoclay layers; this increased the total path of the volatile gases by

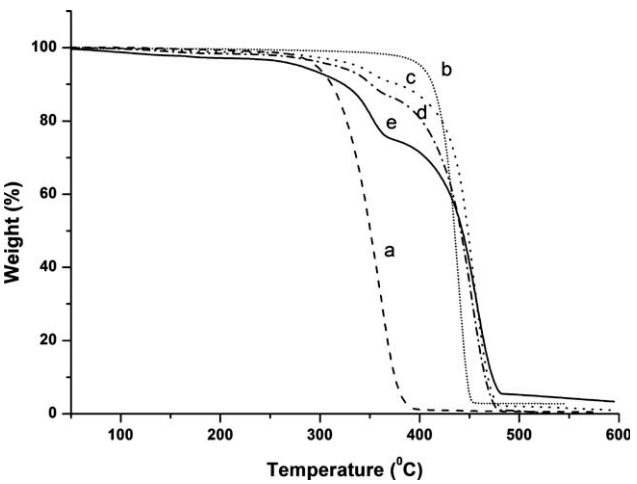

Figure 7 TGA thermograms of (a) PP, (b) OPP, (c) BRPP-10, (d) BRPP-20, and (e) BRPP-30.

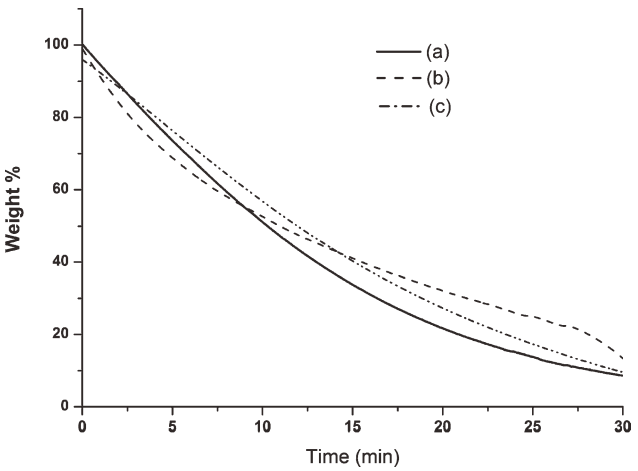

Figure 9 Isothermal TGA thermograms for the (a) PP, (b) OPP, and (c) BRPP-30 nanocomposites at 300°C.

acting as a gas barrier, preventing small gaseous molecules from permeating out of the PP nanocomposites during thermal treatment. At 300°C in a nitrogen atmosphere, the decomposition rate and weight loss of the PP nanocomposites was lower compared to the PP matrix. Furthermore, with the incorporation of 30 wt % banana fiber in the OPP nanocomposites, an increase in weight loss occurred; this was possibly due to the presence of flammable banana fiber. However, the thermal stability of the banana-fiber-reinforced nanocomposites decreased slightly and remained higher compared to virgin PP. Such behavior was probably associated with the morphological changes in proportion with the exfoliated and intercalated nanoclays in the BRPP nanocomposites.

Nonisothermal degradation kinetics

The fundamental rate equation used in all kinetic studies is generally described as

$$\frac{d\alpha}{d\beta} = kf(\alpha) \tag{1}$$

where α is the conversion rate, k is the rate constant, and $f(\alpha)$ is the reaction model, a function depending on the actual reaction mechanism. Equation (1) expresses the rate of conversion ($d\alpha/dt$) at a constant temperature as a function of the reactant concentration loss and rate constant. α is defined as the weight loss at a given temperature, shown as follows:

$$\alpha = \frac{W_0 - W_t}{W_0 - W_f} \tag{2}$$

where W_t, W_0, and W_f are the weight at time t, initial weight, and final weight of the sample, respectively. k is generally given by the Arrhenius equation:

$$k = Ae^{-Ea/RT} \tag{3}$$

where E_a is the apparent activation energy (kJ/mol), R is the gas constant (5.314 J/mol), A is the pre-exponential factor (min^{-1}), and T is the absolute temperature (K). Combining eqs. (1) and (3) gives the following relationship:

$$\frac{d\alpha}{d\beta} = Ae^{-Ea/RT}f(\alpha) \tag{4}$$

Introducing the heating rate (β), that is, the change in absolute temperature with time (dT/dt), for a dynamic TGA process in eq. (4) gives the relationship as follows:

$$\frac{d\alpha}{d\beta} = \frac{A}{\beta}Ae^{-Ea/RT}f(\alpha) \tag{5}$$

Equations (4) and (5) are the fundamental expressions of analytical methods to calculate kinetic parameters on the basis of TGA data. The calculation of E_a from the thermal degradation at different conversion rates during heating is obtained by kinetic analysis with the Kissinger model.[41] In the Kissinger method, $\ln(\beta/T_p^2)$, where T_p is the peak temperature, is plotted against $1/T_p$ for a series of experiments at different heating rates, with the peak temperature obtained from the DTG curve, as shown in the following relationship:

$$\ln\left(\frac{\beta}{T_{p^2}}\right) = \ln\left(\frac{AR}{E_a}\right) + \left(\frac{1}{E_a}\right)\left(\frac{-E_a}{R}\right) \tag{6}$$

Figure 10 shows the linear plots of $\ln(\beta/T_p^2)$ versus $1/T_p$ for the banana-fiber-reinforced OPP nanocomposites from the Kissinger method. Kissinger's method is a special case for determining E_a from a certain conversion rate at the temperature of DTG peak; it may not display the overall trend of E_a. It is shown in Table IV that the E_a values of OPP were found to be much higher than that of the PP matrix because the layered silicates served as a thermal barrier for delaying the hard segments from degradation during the heating process. This observation revealed that clay had an important role in improving the thermal stability of the polymer matrix. This increasing tendency coincided with the thermal analysis results, in which the polymer/nanoclay nanocomposite had a higher thermal stability. With the introduction of banana fiber into the OPP nanocomposites, a two-step thermal decomposition was observed, as per the DTG curve. Thus, in the case of the BRPP nanocomposites, both peak temperatures were considered for the study of E_a. The first degradation stage showed an E_a to about 174.6 kJ/mol, whereas the second gave the value of 185.66 kJ/mol, as shown in the DTG curve. The E_a values during the thermal degradation of the BRPP nanocomposites were found to be higher than that of the virgin PP due to the combined effect of layered silicates and reinforced fiber in the presence of compatibilizer. The E_a calculated from this method provides the information of critical energy needed to initiate a combustion process. The decomposition E_a obtained in this study also helped us greatly to understand the thermal decomposition and stability of the BRPP nanocomposites for their commercial viability.

DSC

The DSC heating and cooling thermograms of the PP, OPP, and BRPP nanocomposites are shown in

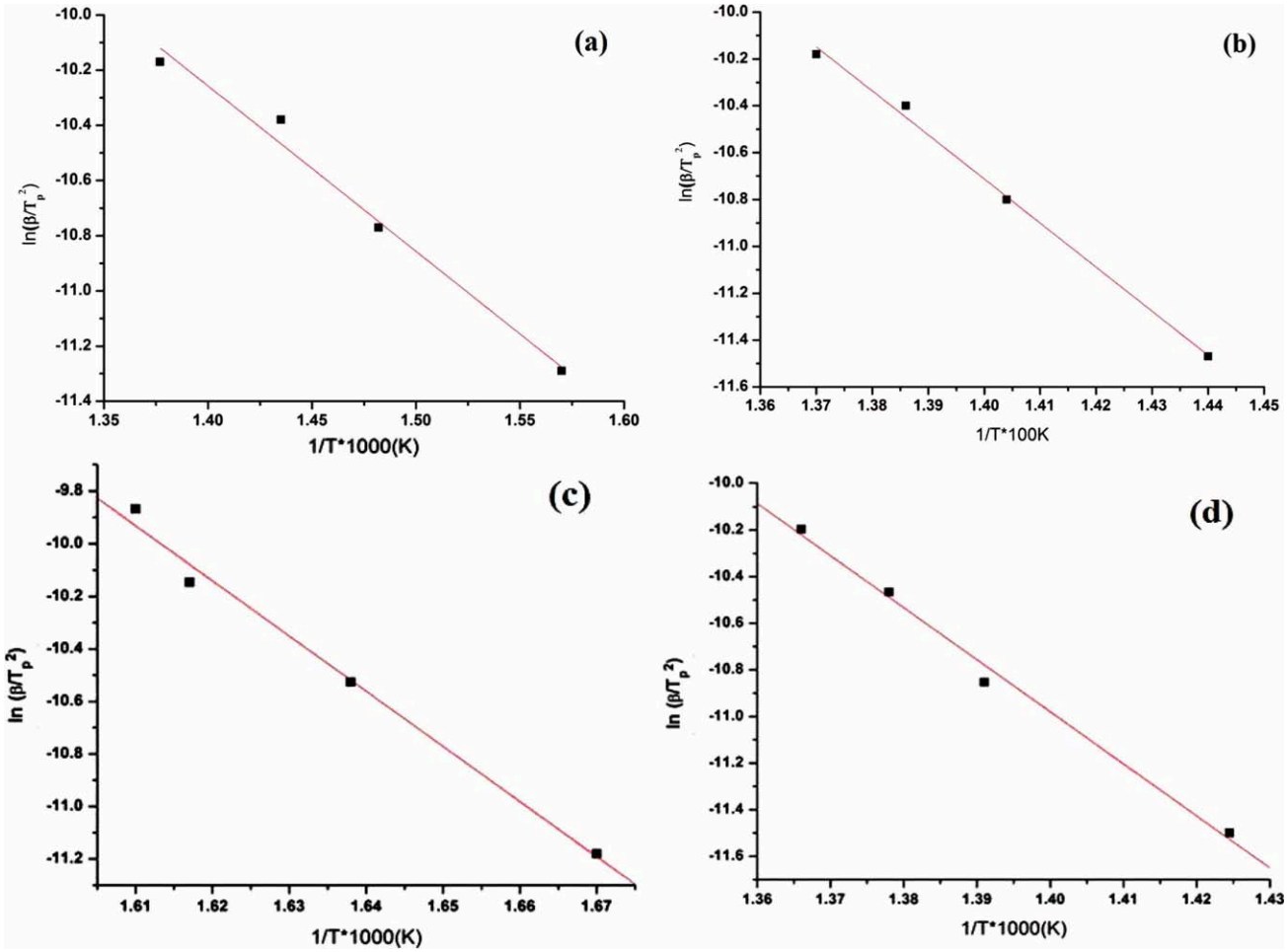

Figure 10 Linear plots of $\ln(\beta/T_p^2)$ versus $1/T_p$ for the (a) PP, (b) OPP, and (c) BRPP-30 nanocomposites first peak. (d) BRPP-30 nanocomposite second peak according to Kissinger's method. [Color figure can be viewed in the online issue, which is available at wileyonlinelibrary.com.]

Figure 11(A, B), respectively. The T_m, T_c, ΔH_m, and X_c values of all of the samples are listed in Table V. Comparing the DSC cooling thermograms of virgin PP with those of the OPP and BRPP nanocomposites, we observed that the T_m of PP was about 162°C, with an X_c value of 29.8%. The incorporation of 5% MA-*g*-PP and 3% nanoclay within the PP matrix resulted in an increase in T_m of about 165.08°C because of the presence of a small amount of polar groups; these promoted promote a nucleating activity during the polymer crystallization and resulted in a moderate increase in T_m, whereas the decrease in X_c to 26.68% suggested a reduction in the perfection of PP crystals. However, we noticed that with the incorporation of banana fiber in the nanocomposites matrix, there was no significant improvement in melting and crystallization. This behavior was probably due to the higher secondary forces arising from the polar groups present in the banana fibers. Also, we ascertained that the banana fibers acted as nucleating sites for PP nanocomposite matrix spherulites, which in turn, accelerated the crystallization rate and enhanced X_c. The X_c values of the PP, OPP, and BRPP nanocomposites were calculated from the following equation:

$$X_c(\%) = (\Delta H_m/\Delta H^*) \times 100\%$$

where X_c is the percentage of crystallinity, ΔH_m is the melting heat of the composite, and ΔH^* is the

TABLE IV
E_a of PP, OPP, and BRPP Nanocomposites Calculated by the Kissinger Method

	First peak		Second peak	
Sample	Adjusted R^2	E_a (kJ/mol)	Adjusted R^2	E_a (kJ/mol)
PP	0.997	124.8		
OPP	0.994	156.3		
BRPP-30	0.996	174.6	0.995	185.66

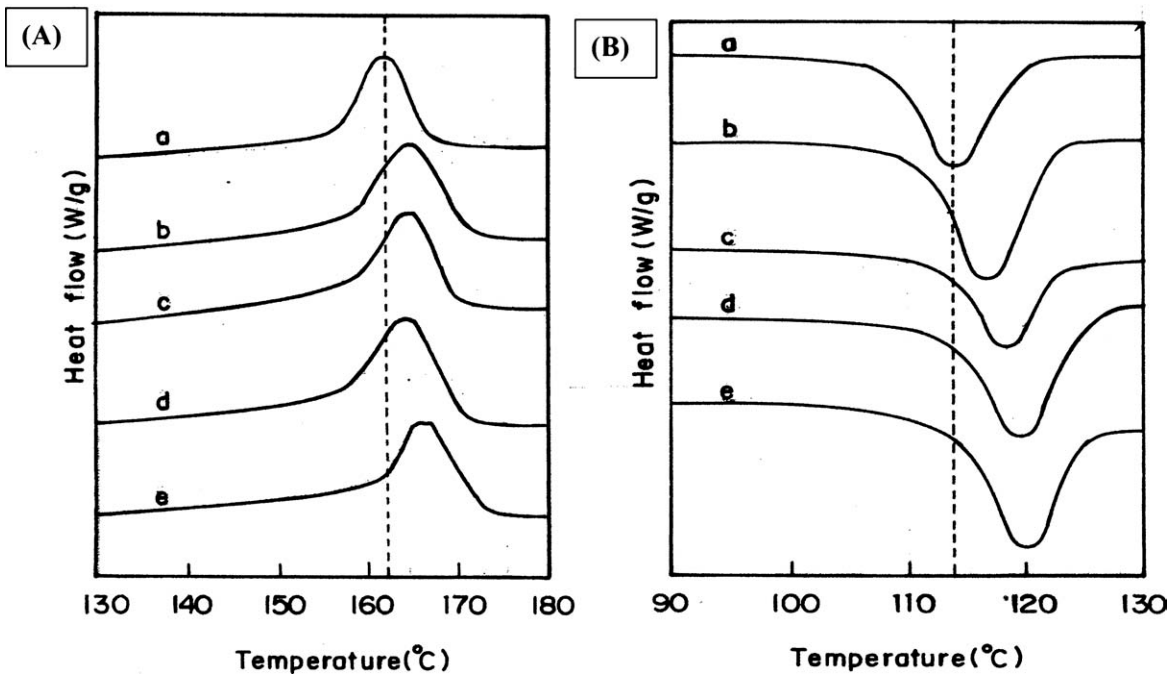

Figure 11 (A, B) DSC (A) heating and (B) cooling curves of (a) PP, (b) OPP, (c) BRPP-10, (d) BRPP-20, and (e) BRPP-30.

heat of the fusion of 100% crystalline PP, which was observed to be 245 J/g according to the literature.[42]

CONCLUSIONS

The mechanical, morphological, thermal, and flammability properties of polypropylene and BRPP nanocomposites were investigated.

- Banana-fiber-reinforced nanocomposites prepared with 3 wt % nanoclay and with a 30 wt % fiber loading in the presence of 5 wt % MA-*g*-PP showed optimum mechanical strength.
- Morphological observations confirmed the efficient dispersion of the nanoclays and intercalation of the polymer segments into the clay galleries in the OPP nanocomposites, which further exhibited an exfoliated structure in the presence of banana fibers.
- TGA thermograms also revealed a higher thermal stability of the reinforced nanocomposites in the presence of nanoclays.
- The flammability study of banana-fiber-reinforced OPP nanocomposites indicated a variation in reaction-to-fire parameters and gave an earlier ignition time compared to virgin PP, whereas the other parameters, such as HRR and average MLR increased with increasing percentage of fiber loading in the nanocomposite matrix.
- DSC measurements also indicated an increased T_c in the BRPP nanocomposites compared with virgin PP; this indicated the nucleating ability of banana fiber during crystallization due to a strong interaction between the nanoclays, fibers, and polymer matrix.

TABLE V
Thermal Properties of the PP, OPP, and BRPP Nanocomposites

Sample	T_m (°C)	T_c (°C)	ΔH_m (J/g)	X_c (%)
PP	162.00	116.54	71.50	29.80
OPP	165.08	116.72	65.38	26.68
BRPP-10	164.04	118.08	147.41	60.16
BRPP-20	164.67	118.81	189.36	77.28
BRPP-30	166.37	120.99	172.96	70.59

References

1. Bledzki, A. K.; Gassan, J. Prog Polym Sci 1999, 24, 221.
2. Yong, L.; Qinglin, W.; Craig, M.; Clemons, Fei, Y.; Yanjun, X. J Reinf Plast Compos 2007, 22, 3959.
3. Thwe, M. M.; Liao, K. Composite 2002, 33, 43.
4. Plackett, D. Presented at the 7th Toronto Conference on Progress in Woodfibre–Plastic Composites, Toronto, Canada, 2002.
5. George, J.; Bhagawan, S. S.; Thomas, S. J Appl Polym Sci 1997, 64, 1121.
6. Devi, L. U.; Joseph, K.; Manikanada Nair, K. C.; Thomas, S. J Appl Polym Sci 2004, 94, 503.
7. Cantero, G.; Arbelaiz, A.; Mugika, F.; Valea, A.; Mondragon, I. J Reinf Plast Compos 2003, 22, 37.
8. George, J.; Bhagawan, S. S.; Thomas, S. J Appl Polym Sci 1997, 64, 1121.
9. Doan, T. T. L.; Gao, S.-L.; Mäder, E. Compos Sci Technol 2006, 66, 952.
10. Joseph, K.; Thomas, S.; Pavithran, C. Polymer 1996, 37, 5139.
11. Samal, S. K.; Mohanty, S.; Nayak, S. K. Polym-Plast Technol Eng 2009, 48, 397.

12. Bin, L.; Jinmei, H. Polym Degrad Stab 2004, 83, 41.
13. Kozlowski, R.; Wladyka-Przybylak, M. Polym Adv Technol 2008, 19, 446.
14. Biswal, M.; Mohanty, S.; Nayak, S. K. J Appl Polym Sci 2009, 114, 4091.
15. Vaia, R. A.; Jandt, K. D.; Kramer, E. J. E.; Giannelis, P. Macromolecules 1995, 28, 8080.
16. Krishnamoorti, R.; Vaia, R. A.; Giannelis, E. P. Chem Mater 1996, 8, 1728.
17. Giannelis, E. P.; Krishnamoorti, R.; Manias, E. Adv Polym Sci 1999, 138, 107.
18. Ray, S. S.; Okamoto, M. Prog Polym Sci 2003, 28, 1539.
19. Ratna, D.; Manoj, N. R.; Varley, R.; Raman, R. K. S.; Simon, G. P. Polym Int 2003, 52, 1403.
20. Mirabella, F. M.; Dekker Encyclopedia of Nanoscience and Nanotechnology; Marcel Dekker: New York, 2004; Vol. 4, p 3015.
21. Lei, Y.; Wu, Q. L.; Clemons, C. M. J Appl Polym Sci 2007, 103, 3056.
22. Joy, K. M.; Hwang, K. J.; Ha, C. S. Polymer 2005, 46, 1995.
23. Dennis, H. R.; Hunter, D. L.; Chang, D.; Kim, S.; White, J. L.; Cho, J. W.; Paul, D. R. Polymer 2001, 42, 9513.
24. Liu, X.; Wu, Q. Polymer 2001, 42, 10013.
25. Wang, K. H.; Choi, M. H.; Koo, C. M.; Choi, Y. S.; Chung, I. J. Polymer 2001, 42, 9819.
26. Gloaguen, J. M.; Lefevre, J. M. Polymer 2001, 42, 5841.
27. Marchant, D.; Jayaraman, K. Ind Eng Chem Res 2002, 41, 6402.
28. Okada, A.; Usuki, A. Macromol Mater Eng 2006, 291, 1449.
29. Bikiaris, D.; Matzinos, P.; Prinos, J.; Flaris, V.; Larena, A.; Panayiotou, C. J Appl Polym Sci 2001, 80, 2877.
30. Mohanty, S.; Verma, S. K.; Tripathy, S. S.; Nayak, S. K. J Reinf Plast Compos 2004, 23, 625.
31. Lei, Y.; Wu, Q. L.; Clemons, C. M. J Appl Polym Sci 2007, 103, 3056.
32. Neilson, L. E. J Macromol Sci 1967, 5, 920.
33. Jeffrey, W. G.; Catheryn, L. J.; Alexander, B. M.; Harris, R., Jr. Chem Mater 2000, 12, 1866.
34. Basch, A.; Lewin, M.; Kirk-Othmer Encyclopedia of Polymer Science and Technology; Wiley: New York, 1977; Suppl. 2.
35. Ryszard, K.; Maria, W. Polym Adv Technol 2008, 19, 446.
36. Kandola, B. K.; Horrocks, A. R.; Composites. In: Horrocks AR, Price D, editors. Fire retardant materials. Cambridge: Woodhead Publishing Ltd, 2002; p 182.
37. Lei, Y.; Wu, Q. L.; Clemons, C. M. J Appl Polym Sci 2007, 103, 3056.
38. Ismail, K.; In Polypropylene: An A–Z Reference; Karger-Kocsis, J., Ed.; Kluwer Academic: Dordrecht, The Netherlands, 1999; p 783.
39. Razdan, S.; Patra, P. K.; Warner, S. Polym Mater Sci Eng 2003, 69, 722.
40. Usuki, A.; Kojima, Y.; Okada, A.; Fukushima, Y.; Kurauchi, T.; Kamigaito, O. J Mater 1993, 8, 1185.
41. Kissinger, H. E. J Res Natl Bur Stand 1956, 57, 217.
42. Kumar, S. Wood Fiber Sci 1994, 26, 270.